Novel 3D-Printed Reconfigurable Origami Frequency Selective Surfaces With Flexible Inkjet-Printed Conductor Traces

Yepu Cui, Syed Abdullah Nauroze, Manos M. Tentzeris

School of Electrical and Computer Engineering
Georgia Institute of Technology
Atlanta, Georgia, 30332
E-mail: yepu.cui@gatech.edu

Abstract — **This work outlines the first-of-its-kind integration of 3D and inkjet printing additive manufacturing processes for the realization of tunable origami structures. The outcome of this process demonstrated a tremendous structural strength improvement over paper-based origami structures, also featuring very good potential for more complicated origami-inspired designs. A mm-wave 4D tunable Miura-shaped frequency selective surface (FSS) is demonstrated using this process. This FSS shows both frequency and bandwidth tunability, and has excellent angle of incidence rejection.**

Keywords — **origami, 3D printing, inkjet printing, additive manufacturing, frequency selective surface, Miura, flexible.**

I. INTRODUCTION

Origami is the art of paper folding. Introducing origami structures into microwave design enables unprecedented capabilities for continuous-range tunability. Currently, most of the origami inspired microwave components such as antennas, frequency selective surfaces (FSS) have been realized on paper-based substrates [1]-[3]. While paper is ideal for realizing proof of concept origami-inspired structures, it is prone to absorb moisture, tear and features high dielectric losses. Moreover, paper-based origami RF structures need to be folded manually that limits their use in mm-wave applications when components become very small. Therefore, it is imperative to device a fully automated fabrication process with durable and weather resistant materials to realize the origami-inspired structures in real-life and mm-wave applications.

This paper builds on the previous research of [1] by introducing 3D and inkjet printing technology into a reconfigurable mm-wave Miura frequency selective surface (M-FSS). Fully 3D printed flexible substrates eliminate the requirement of folding and cutting which enables more complicated design elements such as slots, round holes, etc. Meanwhile, fully automated high-accuracy fabrication methodology can produce smaller units which opens the potential for 5G and mm-wave applications. Also the additively manufactured substrate shape or thickness is fully customizable depending on the application scenarios, so the M-FSS can be easily transformed into other components such as absorbers, multilayer FSS or curved FSS.

The proposed 3D-printed M-FSS structure is a mm-wave special filter that has inkjet printed flexible dipole elements.

The dipole elements are printed on bridge-like structures which reduce the mechanical stress around the fold line as the M-FSS structure is folded [1]. The proposed M-FSS structure facilitates wideband tunability with good angle of incidence (AoI) rejection.
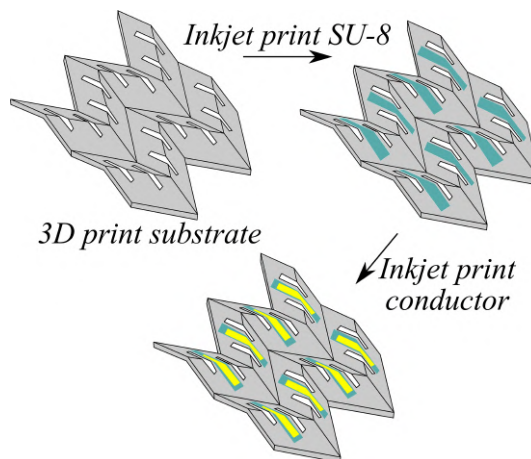

Fig. 1. Fabrication process for 3D printed origami structures.

II. FABRICATION PROCESS

The three-step fabrication process is shown in Fig. 1 that contains: First, 3D print dielectric substrate. Then inkjet print a thin SU-8 buffer to smooth out the substrate surface. Finally inkjet print the conductive layers and sinter with a low temperature gradient.

A. 3D Printed Dielectric Substrate

The Miura structure is printed using Formlabs Form 2 Stereolithography (SLA) 3D printer. SLA is an optical based 3D printing technology that uses laser or optical projector as the energy source to cure and solidify light sensitive resin layer-by-layer to realize complex 3D structures. The resolution is typically limited by the source optics, thereby making it a superior candidate for mm-wave applications as compared to other 3D printing technologies such as Fused Deposition Modeling (FDM) [4]. To date, commercialized SLA resins feature a wide variety of hardness, colors and RF characteristics. The features of flexible elastomer resin makes it an ideal origami substrate replacement for
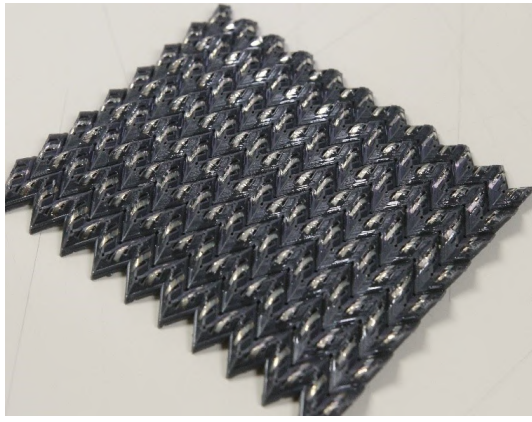
Fig. 2. Finished 3D/inkjet printed tunable Miura shape FSS.

paper. The utilized material is Formlabs Flexible (FLGR02) photopolymer. This flexible material is a rubber-like elastomer with tensile strength of 7.7-8.5 MPa with 80% elongation and 50 um maximum resolution [5]. The characterized dielectric constant at 22 GHz is 2.78 with loss tangent 0.03 [6]. A finished 8x10 Miura FSS is shown in Fig. 2.

The substrate is printed with 50 um layer thickness, and post processed using Formlabs wash and cure system. The automated isopropyl alcohol washer with magnetic stirrer and timer is used to remove extra resin left on samples surface. The curing system has 405 nm LED lights and a heater to ensure the best structure strength. With wash-and-cure post processing, 3D printed substrate will have less chance of failure, smoother surface, more consistency and less electromagnetic losses due to improved cross link by UV exposure at heated plate. The wash time used for Flexible resin is 15 minutes with 99% isopropyl alcohol, while the cure time is 20 minutes at 60°C.

B. Inkjet Printed Buffer Layers

With 50um high resolution 3D printing and optimized post processing, substrate can demonstrate a relatively smooth surface, but compared to the 0.8um thickness of one layer silver nanoparticle (SNP) conductor, the 3D printed substrate still has a relatively rough surface. Therefore, six layers of MicroChem SU-8 are inkjet printed to minimize its surface roughness [7]. As shown in Fig. 3 the substrate surface roughness, especially on curved area, has been dramatically improved by SU-8 buffer layers.

C. Inkjet Printed Conductor Traces

The dipoles are inkjet-printed with SunChemical EMD5730 silver nanoparticle (SNP) ink using Dimatix 2800 inkjet printer with 20 um drop space (1270 dpi). Meanwhile, to improve the SNP ink adhesion, 90 seconds of ultraviolet (UV) ozone treatment is adopted before printing the conductor traces.

There are two challenges to print the conductors. Firstly, as the conductor is printed on a 3D substrate with a 2D pattern, the actual drop spacing density or drops per inch (DPI) will

be compromised on 3D structures. The reason being is that fixed printing nozzles are usually parallel to a 2D flat substrate instead of a 3D one, meaning that the 2D pattern is projected onto the 3D shape. For a 3D substrate, the printing area is a ramp that is not parallel to the fixed printing nozzles. In this situation, the actual printed 3D trace is longer than the 2D length of the pattern, this will cause a DPI loss by a factor of $\sin(\theta)$ (θ is the angle between printing head and substrate). For example, the printed sample in Fig.2 has a ramp with 35° maximum angle, so at least 20% more layers are needed to compensate the resolution losses. With a series testing, six layers of silver printing is adopted for this design.

The second challenge is the fact that SNP inks need relatively high temperature sintering, typically above 150°C, commonly 180°C for best conductivity and adhesion. But the high temperature will damage the 3D printed substrate. Placing the substrate at 150°C for 30 minutes will dramatically reduce its elasticity so the substrate will break after few folds. Additionally, the substrate will shrink under high temperatures leading to cracks on conductor traces which will make them discontinuous and unusable (Fig. 4a). To solve this problem, a low temperature gradient sintering process is developed. After SNP printing, the sample was placed on a hot plate ramping from room temperature to 90°C with 150°C/hr temperature ramp, and hold at 90°C for 30 minutes to dry the pattern completely. Then, increase the temperature from 90°C to 120°C with 150°C/hr ramp, hold at 120°C for 15 minutes to sinter the pattern without breaking substrate. Finally, the hot plate was turned off so as to let the sample slowly cool back to room temperature to avoid deformation caused by sudden temperature change.

With this low temperature gradient sintering process, the conductor quality is greatly improved and the realized conductor trace shows a conformal and smooth surface (Fig. 4b) on a curved 3D substrate. The measured sheet resistance using four-point probe test method is 0.02 Ω/sq which is identical to the high temperature sintering results on a heat stabilized substrate.
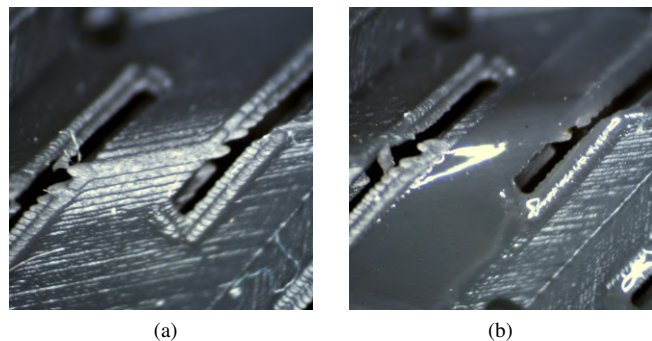

(a)　　　　　　　　　　(b)

Fig. 3. Comparison of SU-8 surface modification (a) rough surface on curved area; (b) smooth surface with SU-8 buffer layer.

III. 3D Printed Miura FSS

A. Design

A single Miura unit is shown in Fig. 5a and Fig. 5b. The size of each element is reduced dramatically to 7x5mm compared with previous research that used elements around 20x20mm [1]. The reduced size and thicker substrate make it especially challenging to produce a foldable Miura FSS because the bending force applied on each foldline may break the substrate as well as the conductor traces. For example, the intersection of the foldlines will have stresses from three different directions applied on this single point; the substrate may break from this point during folding. In this design, a stress release hole (Fig. 5b) with 0.4mm radius is introduced to each foldline intersection to release the applied stresses. However, even with optimized low temperature sintering process for the conductor traces, they may states crack under strong bending stress. To enable more folding spaces, two slots are introduced by the edge of each conductor to form a bridge-like structure (Fig. 5b). The bridge-like structure can transform bending stress to rotating stress, which will improve the overall flexibility for each trace [1]. Moreover, every sharp edge on the bridge-like structures are smoothened with a 2 mm radius round transition that will further increase the flexibility of the conductors.

B. Simulation and Measurement

This Miura FSS was designed and simulated in Ansys Electronics Desktop with HFSS design. The simulation setup uses master and slave boundaries along with Floquet port excitations. This environment will simulate the FSS as infinitely large but only needs one element, dramatically reducing the simulation time. The simulated results were verified on the measurement setup shown in Fig. 6. A 3D printed frame and laser cut acrylic holder was made to compress and rotate the sample.
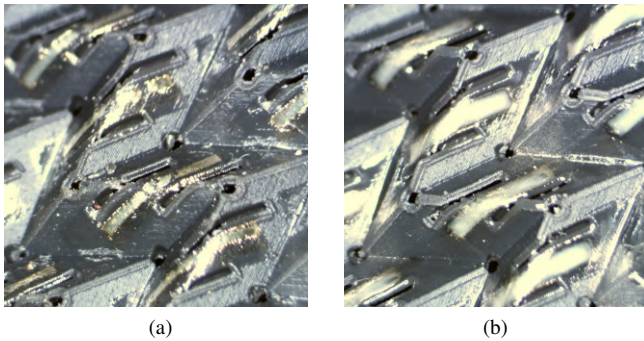

Fig. 4. Comparison of sintering condition (a) high temperature sintering; (b) low temperature gradient sintering.
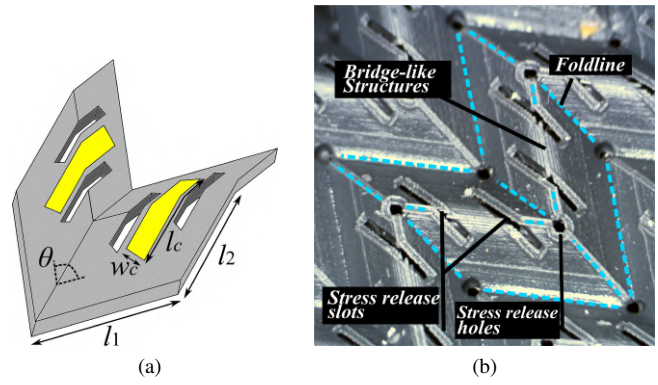

Fig. 5. Single Miura unit (a) a optimized Miura unit with l_1=5mm, l_2=7mm, θ = 110°, w_c=1mm, l_c=6mm, substrate thickness=0.8mm; (b) 3D printed Miura unit with stress release design.
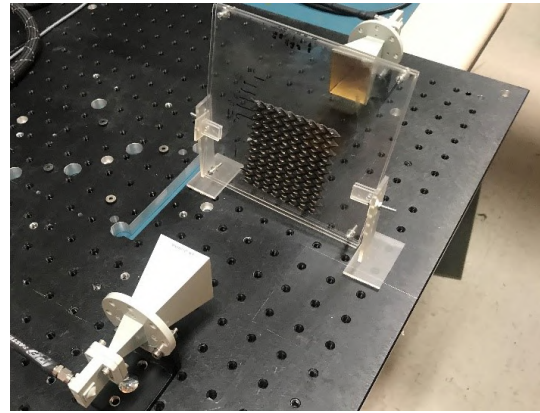

Fig. 6. Measurement setup with sample frame and holder.

The simulated and measured insertion loss of the Miura FSS with respect to different angle of incidence (AoI) is shown in Fig. 7. The -10dB bandwidth increase significantly from 14% to 32% by the increased AoI from 0° to 60°. The bandwidth change is caused by increased equivalent circuit terminal resistance R_A with larger angles of incidence η, the function of R_A respect to η is shown in (1). Note that Z is the intrinsic impedance for 3D printed material, D_x, D_z is FSS element spacing along x and z axis, Δ_l is the transmitted power. As shown in (2), the reflection coefficient Γ will increase with R_A, which will boost the insertion loss that results in an improved percentage bandwidth [8].

$$R_A = \frac{Z}{2D_x D_z} \frac{\Delta_l^2}{cos(\eta)} \sim \frac{1}{cos(\eta)} \tag{1}$$

$$|\Gamma| = \left| \frac{-1}{1 + jX_A/R_A} \right| \tag{2}$$

Fig. 7. Frequency response of M-FSS(θ=110°) for different values of angle of incidence.

Fig. 8. Frequency response with different values of folding angle θ.

The simulated and measured insertion loss of the Miura FSS for different folding angles(θ=110°,90°,80°,60°) are shown in Fig. 8. From this figure, it is clear that resonant frequency shifts higher as the folding angle decreases. The frequency shift is caused by reduced effective conductor length due to the folding. The measured frequency shift matches closely to the simulated results, but the measured value of insertion loss decreases with smaller folding angles. This is because the simulation considers FSS as infinitely large, so unfolded 10x8 Miura FSS (50x60mm) will cover the whole antenna aperture which can be considered as infinity large. Nevertheless, the size of folded 10x8 Miura FSS will reduce to 50x7mm(θ=60°) which cannot cover the entire illuminating antenna beamwidth anymore. The finite FSS introduces edge currents which lead to leakage that reduces insertion loss [9]. The tested 10x8 Miura FSS substrate is the largest printable size for the utilized 3D printer.

IV. Conclusion

This paper demonstrated the first-of-its-kind additive manufacturing process for 3D printed prototype with origami-based RF devices. The fabricated mm-wave M-FSS with this process shows great resonance frequency and bandwidth tunability as well as excellent AoI rejection. The proposed process features a unique capability to realize more rugged and more complicated origami-inspired designs for real-world applications up to mm-wave and sub-THz frequency ranges. It also enables more application scenarios for the M-FSS such as integration with 3D printed microfluidics, multi-layer configurations, beam steering with customized 3D curve and cut configurations, etc.

References

[1] S. A. Nauroze L. Novelino M. M. Tentzeris G. H. Paulino, "Inkjet-printed 4d tunable spatial filters using on-demand foldable surfaces", *2017 IEEE MTT-S International Microwave Symposium (IMS)*, pp. 1575-1578 June 2017.

[2] Xueli Liu, Shun Yao, S. V. Georgakopoulos, B. S. Cook and M. M. Tentzeris, "Reconfigurable helical antenna based on an origami structure for wireless communication system", *2014 IEEE MTT-S International Microwave Symposium (IMS2014)*, Tampa, FL, 2014, pp. 1-4.

[3] X. Liu, S. Yao and S. V. Georgakopoulos, "Mode reconfigurable bistable spiral antenna based on kresling origami", *2017 IEEE International Symposium on Antennas and Propagation & USNC/URSI National Radio Science Meeting,*, San Diego, CA, 2017, pp. 413-414.

[4] R. Bahr, X. He, B. Tehrani and M. M. Tentzeris, "A Fully 3D Printed Multi-Chip Module with an On-Package Enhanced Dielectric Lens for mm-Wave Applications Using Multimaterial Stereo-lithography,", *2018 IEEE/MTT-S International Microwave Symposium - IMS*, Philadelphia, PA, 2018, pp. 1561-1564.

[5] Using Flexible Resin [Online]. Available: https://support.formlabs.com/s/article/Using-Flexible-Resin

[6] T. Lin, R. Bahr, M. Tentzeris, R. Pulugurtha, V. Sundaram and R. Tummala, "Novel 3D-/Inkjet-Printed Flexible On-package Antennas, Packaging Structures, and Modules for Broadband 5G Applications," 2018 IEEE 68th Electronic Components and Technology Conference (ECTC), San Diego, CA, 2018, pp. 214-220.

[7] W. Su, S. A. Nauroze, B. Ryan and M. M. Tentzeris, "Novel 3D printed liquid-metal-alloy microfluidics-based zigzag and helical antennas for origami reconfigurable antenna trees," 2017 IEEE MTT-S International Microwave Symposium (IMS), Honolulu, HI, 2017, pp. 1579-1582.

[8] B. A. Munk, "Frequency selective surfaces theory and design. john wiley&sons," 2000.

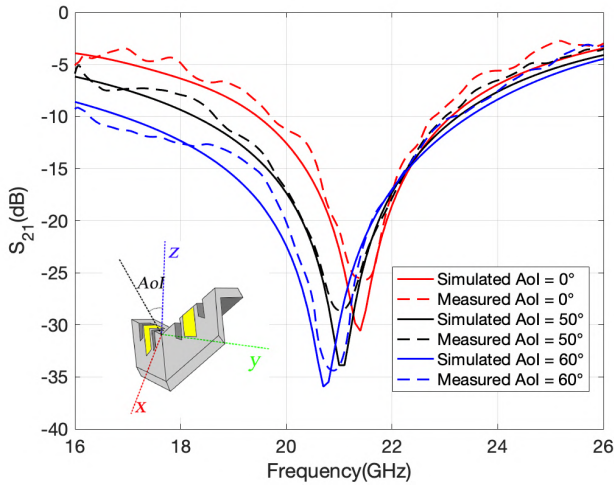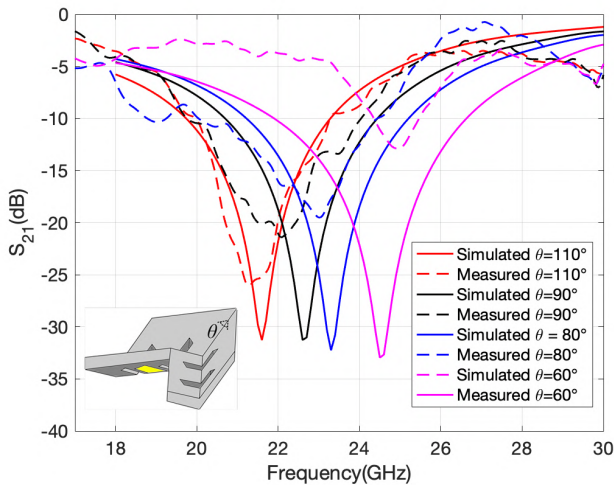[9] B. A. Munk, "Finite Antenna Arrays and FSS. john wiley&sons," 2003.